## ARTICLE

Check for updates

# Size dependent nature of the magnetic-field driven superconductor-to-insulator quantum-phase transitions

Xiaofu Zhang [1✉], Adriana E. Lita[2], Huanlong Liu[1], Varun B. Verma[2], Qiang Zhou [3], Sae Woo Nam[2] & Andreas Schilling [1✉]

The nature of the magnetic-field driven superconductor-to-insulator quantum-phase transition in two-dimensional systems at zero temperature has been under debate since the 1980s, and became even more controversial after the observation of a quantum-Griffiths singularity. Whether it is induced by quantum fluctuations of the superconducting phase and the localization of Cooper pairs, or is directly driven by depairing of these pairs, remains an open question. We herein experimentally demonstrate that in weakly-pinning systems and in the limit of infinitely wide films, a sequential superconductor-to-Bose insulator-to-Fermi insulator quantum-phase transition takes place. By limiting their size to smaller than the effective penetration depth, however, the vortex interaction alters, and the superconducting state re-enters the Bose-insulating state. As a consequence, one observes a direct superconductor-to-Fermi insulator in the zero-temperature limit. In narrow films, the associated critical-exponent products diverge along the corresponding phase boundaries with increasing magnetic field, which is a hallmark of the quantum-Griffiths singularity.

[1] Department of Physics, University of Zürich, Zürich, Switzerland. [2] National Institute of Standards and Technology, Boulder, CO, USA. [3] Institute of Fundamental and Frontier Sciences, University of Electronic Science and Technology of China, Chengdu, Sichuan, China. ✉email: zhang@physik.uzh.ch; schilling@physik.uzh.ch

Superconductivity in strong magnetic fields has been one of the fundamental problems from both the theoretical and practical point of views since its discovery. The superconducting state is a macroscopic quantum state, which is phenomenologically characterized by dissipationless electric currents and the Meissner effect. According to the Bardeen, Cooper Schrieffer theory, superconductivity originates microscopically from coherently paired electrons (Cooper pairs)[1]. The superconducting state is therefore characterized by a complex order parameter with an amplitude (related to the Cooper pair density $n_s$ or the energy gap $\Delta$) and a phase $\phi$. The destruction of the superconducting state in high magnetic fields can occur through the suppression of $n_s$ to zero. However, phase fluctuations of the order parameter can also destroy the zero-resistance state[2]. When the external field exceeds the lower-critical field in type-II superconductors, the magnetic field enters the superconductors via quantized flux lines (vortices). Sufficiently mobile vortices, as a manifestation of phase fluctuations, may generate dissipation and can drive superconductors into normal conductors.

The magnetic field-driven superconductor-to-insulator transition (SIT) in thin films at zero temperature is a well-documented quantum phase transition[3–5] and has been observed in a myriad of experiments[6–16]. A long-standing controversy is the question whether the SIT is due to the loss of long-range coherence of $\phi$ (bosonic scenario) or due to the breaking of Cooper pairs that suppresses $n_s$ to zero (fermionic scenario)[3–5]. The bosonic scenario describes the SIT as a result of quantum phase fluctuations, in which the superconducting and the insulating states are separated by a single quantum critical point[14,17,18]. In the superconducting state, the Cooper pairs are mobile and the vortices are localized into a vortex lattice or glass, whereas in the insulating state, the vortices are mobile but the Cooper pairs are localized into isolated superconducting islands, forming a Bose-insulating state[19,20]. By contrast, the SIT in the fermionic scenario is thought to be driven by the destruction of Cooper pairs and the localization of charge carriers in high-enough fields, thereby forming a Fermi insulator[21–23]. Despite the majority of experiments demonstrating a quantum fluctuation-induced superconductor-to-Bose insulator quantum phase transition[7–9,14,24,25], a direct superconductor-to-Fermi insulator quantum phase transition that is induced by the breakdown of Cooper pairs has also been reported[10,11,26].

Moreover, recent observations in crystalline quasi-two-dimensional (2D) and one-dimensional (1D) superconducting systems revealed a quantum Griffiths singularity[27–33], which is experimentally characterized by divergent critical-exponent products of the dynamical critical exponent and the correlation length exponent $z\nu$. This phenomenon is attributed to quenched-disorder effects at the transitions, despite the fact that origin of such quenched disorder in clean systems is somewhat obscure[27–32,34,35]. The quantum Griffiths singularity offers a new perspective on the nature of the SIT or metal-to-insulator transitions, but also evokes a fundamental problem, namely the apparent lack of universality in experiments probing superconductor-to-insulator quantum phase transitions[3–16,21–33].

Due to the weak pinning in amorphous superconductors, the manifestation of intrinsic vortex interactions can be directly probed and they therefore represent an optimal platform to study vortex-related phase transitions. Depending on the bridge width $w$, we observe all of the above mentioned magnetic field-induced phenomena in thin amorphous superconducting films, such as superconductor-to-Bose insulator quantum phase transitions, direct superconductor-to-Fermi insulator phase transitions, and a quantum Griffiths singularity. Our results can therefore, in part, explain the seeming absence of universality of these transitions.

## Results and discussion

**Preparation and characterization of the WSi bridges.** We fabricated a series of superconducting microbridges on a single $10 \times 10$ mm$^2$ amorphous WSi thin film with thickness $d = 4$ nm[36,37], spanning the range of bridge widths $w$ over almost three decades from 2 to 1000 μm. The amorphous nature of our films is illustrated in Fig. 1a. Standard four-electrode transport measurements taken in zero magnetic field on the as-grown films and on the fabricated long bridges are shown in Fig. 1b. To make the results for the different bridge widths comparable, all measurements were performed with the same low current density $j = 1.25$ MA m$^{-2}$, which is around four orders of magnitude below the depairing critical-current density. The respective transition temperatures $T_c(0)$ are all $\approx 3.45$ K, demonstrating the homogeneity and quality of the bridges.

**Phase diagram for infinitely wide films.** The Fig. 1c–f show the sheet resistances $R_s(T)$ for the 1000, 50, 10, and the 2 μm-wide bridges at various magnetic fields near the SIT. The widest bridge (Fig. 1c) shows a well-defined quantum critical field at $B_c^1 = 5.42$T that separates the zero-temperature superconducting state with $\partial R_s / \partial T > 0$ from the insulating state with $\partial R_s / \partial T < 0$. We note that the critical sheet resistance ($R_s \approx 547$ Ω with $\partial R_s / \partial T = 0$ at $B_c^1$ in these 4 nm-thick WSi films is one order-of-magnitude lower than the quantum resistance for Cooper pairs, which is likely due to a fermionic conducting channel of unpaired electrons[8]. Above $B_c^1$, superconducting fluctuations still exist on the insulating side up to $B_c^2 \approx 6.4$T at $T_c(0)$, which supports the scenario of a localization of Cooper pair-induced SIT, i.e., a superconductor-to-Bose insulator quantum phase transition[14]. The $R_s(T)$ on the insulating side between $B_c^1$ and $B_c^2$ are separated by minima $T_{min}(B)$ into two distinct regimes: a regime with superconducting fluctuations and $\partial R_s / \partial T > 0$ for $T > T_{min}(B)$, and a zero-temperature insulating regime with $\partial R_s / \partial T < 0$ (see Fig. 2a, full red circles), thereby defining the phase boundary between the superconducting and the Bose-insulating state. It is interesting to note that a pronounced gap structure has been found in the tunneling spectra of disordered MoC films far above the respective $B_c^1$[38], although a direct relation to the existence of Cooper pairs has not been made. An ultimate proof for the existence of separated superconducting regions in this proposed Bose-insulating phase could only be provided a spectroscopic scanning-tunneling microscopy investigation as carried out in refs. [39,40]. Within our scenario, the localized Cooper pairs in the Bose-insulating regime finally delocalize with increasing temperature at $T_{min}(B)$, leading to a state with finite-temperature superconducting fluctuations. With increasing magnetic field, the $T_{min}(B)$ plateaus monotonically shift from the zero-temperature quantum critical point at $B_c^1(0)$ to $T_c(0)$ at $B_c^2$, the highest temperature where Cooper pairs can persist in the 2D superconducting system on the Bose-insulating side. Similar results were also observed for the 500 μm-wide bridge (Supplementary Fig. 1b), essentially representing the universal properties of infinite 2D superconducting systems.

**Narrowing down the systems size.** As soon as the bridge width $w$ is further reduced, we fail to identify a quantum critical regime down to zero temperature. Already for the 200 μm-wide bridge (Supplementary Figs. 1c and 2b), the $R_s(T)$ shows a downturn with decreasing temperature near $B_c^1$, instead of a temperature-independent value in the zero-temperature limit as we observed it in the wider bridges. By carefully checking all these downturns in $R_s(T)$ shown in Fig. 1 and in the Supplementary Figs. 1 and 2, we
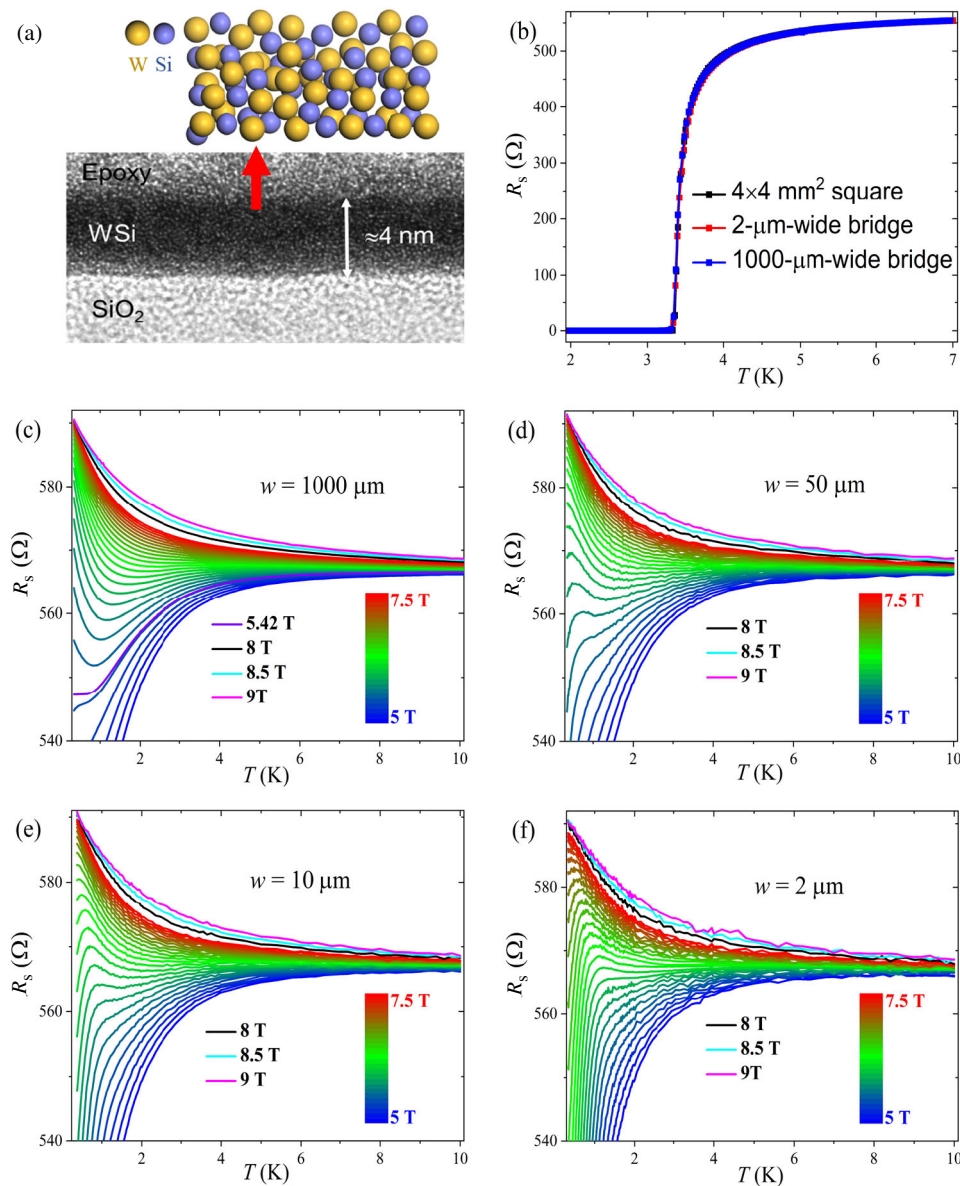
**Fig. 1 Superconductor-to-insulator quantum phase transitions. a** Schematic view of the amorphous WSi films. The amorphous nature and the thickness are examined by cross-sectional transmission electron microscopy. **b** Zero-field normal-to-superconductor transitions of the bare films and the microbridges. **c** Sheet resistance $R_s(T)$ as a function of temperature $T$ in magnetic fields from $B = 5$ to 9 T of the 1000 μm-wide bridge. The violet line shows the separatrix at the quantum critical field $B_c^1$ for the superconductor-to-Bose insulator quantum phase transition. **d–f** Corresponding $R_s(T)$ data of the 50, 10, and the 2 μm-wide bridges, respectively.

find that superconductivity recovers above $B_c^1$ in the narrow bridges, i.e., the initially Bose-insulating state turns into the superconducting state again. When cooling these bridges down from the normal state (see Fig. 2b for the $R_s(T)$ of the 20 μm-wide bridge in 6 T as an example), superconducting fluctuations appear around 6 K with $\partial R_s/\partial T > 0$ at first; then, the $R_s(T)$ curves reach a minimum, similar to those in the wide bridges, corresponding to a finite-temperature superconductor-to-Bose insulator phase transition. The Bose-insulating state with $\partial R_s/\partial T < 0$, however, does not persist down to the zero-temperature limit, but is terminated by re-entering into the superconducting state with $\partial R_s/\partial T > 0$. This "re-entrant" behavior is clearly a size-induced effect, as all the bridges were prepared from the same film. It can therefore not be ascribed to, e.g., chemical disorder or granular effects[41], which should be equally present in all the bridges, irrespective of their width.

Figure 1d–f show the $R_s(T)$ of 50, 10, and 2 μm-wide bridges in the same field range as in Fig. 1c for the 1000 μm-wide bridge, demonstrating that the SIT is completely different from that in the infinite 2D systems. Distinct from the SIT in Fig. 1c, the $R_s(T)$ in the zero-temperature limit drop dramatically with decreasing temperature. The complete evolution of the SIT as a function of bridge width is shown in the Supplementary Fig. 1 and in Supplementary Movie 1. The corresponding phase boundaries between the superconducting and the insulating states (Fig. 2c–e) are well separated by a finite-temperature maximum $T_{max}$ on the $R_s(T)$ curves (open red circles) and the $dR_s(T)/dT$ changes its sign at a characteristic critical field $B_c^*(T_{max})$ (Fig. 2b). With increasing $B$, the corresponding $T_{max}$ plateaus shift monotonically down to zero temperature.

To better visualize the recovery of superconductivity in the Bose-insulating state, Fig. 3 compares representative $R_s(T)$ curves
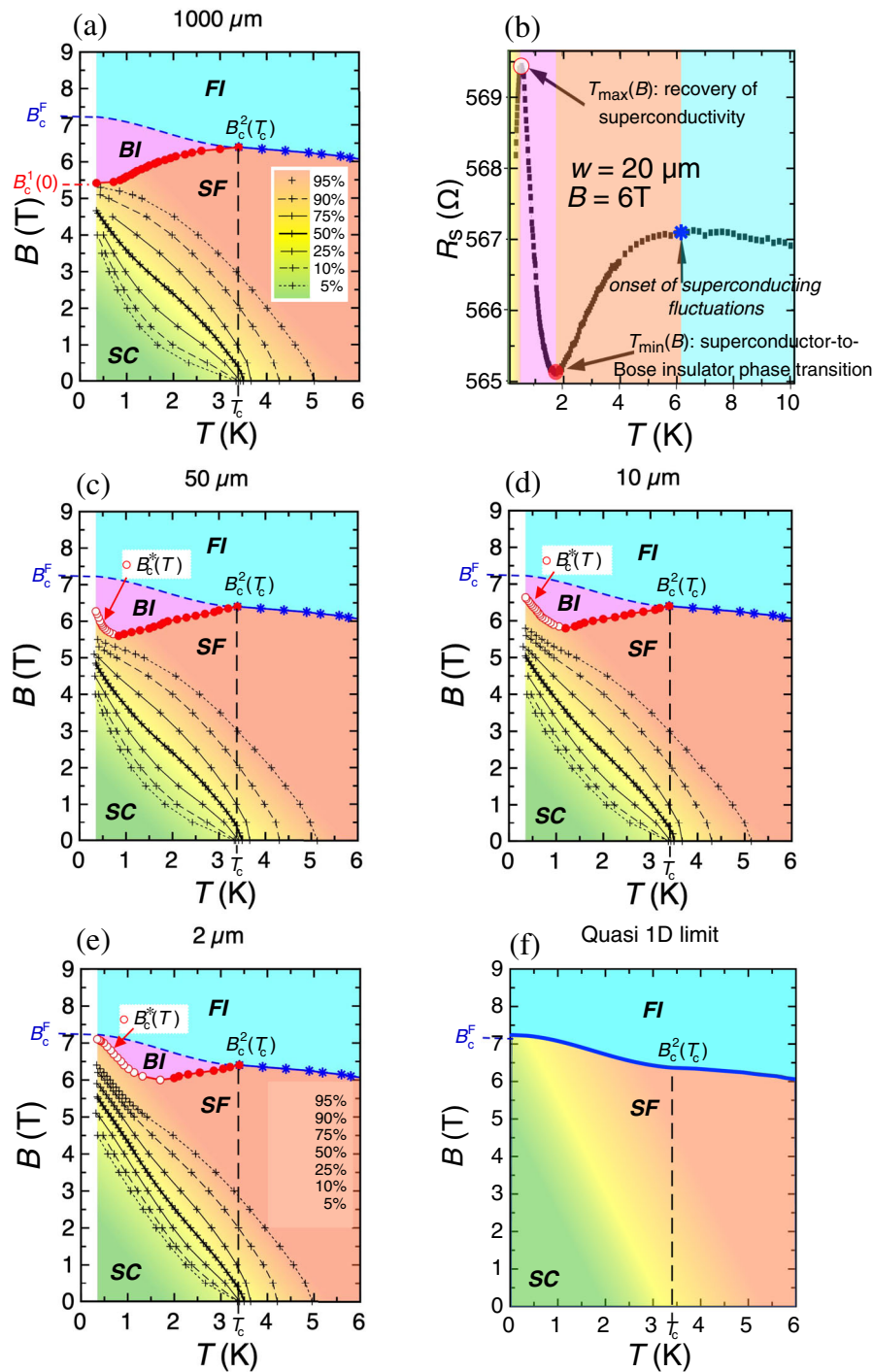
**Fig. 2 The schematic magnetic field $B$ vs. temperature $T$ phase diagrams. a** Sequential superconductor (SC)-Bose insulator (BI), -Fermi insulator (FI) quantum phase transitions for infinite 2D superconducting systems. The lines connecting the crosses (+) represent the measured resistance values for fixed fractions of the normal-state resistance from 5% to 95%, extending to the region dominated by superconducting fluctuations (SF). **b** Sheet resistance $R_s(T)$ from 0.35 to 10 K in $B = 6$ T for the 20 µm-wide bridge as an example. All relevant temperatures are marked with arrows. The coloring of the respective phases and the symbols marking the phase transitions between them are the same as we used in the phase diagrams in Fig. 2a, c–e and in the Supplementary Figs. 5, 8, and 9. **c–e** Superconductor-to-insulator phase transitions for quasi-2D superconducting systems with dimensions smaller than the Pearl length $\Lambda(0)$. The blue stars indicate the onset of the superconducting fluctuations; the full red circles represent the temperatures $T_{min}(B)$ in the sheet-resistance $R_s(T)$ data, whereas the open red circles are determined by the respective $T_{max}(B)$ in $R_s(T)$, signaling the recovery of superconductivity in the narrow bridges. All these definitions are visualized in Fig. 2b and in the Supplementary Figs. 8 and 9. The dashed blue line ending at the Fermi insulator quantum critical field $B_c^F$ schematically separates the Bose-insulating and the Fermi-insulating states, with a qualitatively much more pronounced divergence of $dR_s/dT$ towards zero temperature in the former than in the latter state (see also Supplementary Figs. 8 and 9). **f** Expected superconductor-to-insulator phase transition for systems approaching the 1D limit.
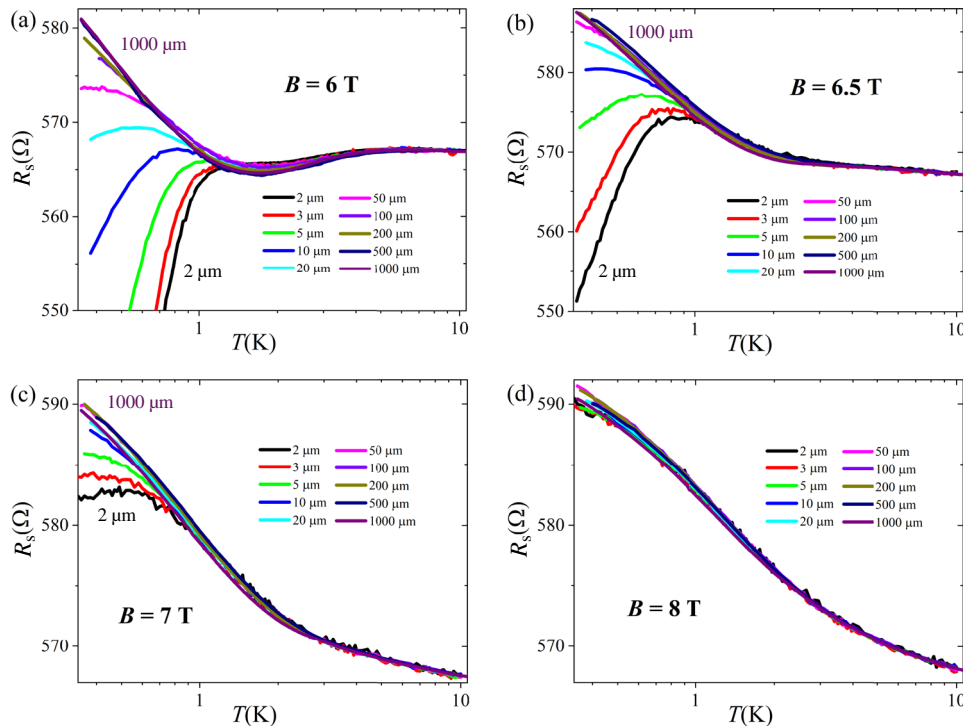
**Fig. 3 Recovery of superconductivity in magnetic fields between the Bose insulator quantum critical field $B_c^1 = 5.42\,T$ and the Fermi insulator quantum critical field $B_c^F = 7.25\,T$ upon decreasing the bridge width. a–d** Sheet-resistance $R_s(T)$ curves of all the bridges taken in magnetic fields $B = 6, 6.5, 7$, and 8 T, respectively.

for all the bridges in magnetic fields $\gtrsim B_c^1$ up to 8 T. Despite a $T_{min}$ for fields between $B_c^1$ and $B_c^2$ (Fig. 3a) is observed for all bridges in $B = 6$ T (i.e., a superconductor-to-Bose insulator transition), the $R_s(T)$ curves show a dramatic decrease in the narrow bridges in the low-temperature limit, suggesting that the freely mobile vortices in the originally Bose-insulating state are re-pinned. By further increasing the magnetic fields above $B_c^2$, the superconductor-to-Bose insulator transition at $T_{min}$ is entirely absent for all bridges. The recovery of superconductivity in the narrow bridges, however, still persists, indicating a direct superconductor-to-Fermi insulator quantum phase transition in the zero-temperature limit (Fig. 3b, c). At sufficiently high fields ($B = 8$ T), where electrons cannot condense into Cooper pairs even at $T = 0$, the $R_s(T)$ curves do not exhibit any size effects (Fig. 3d).

We have also carefully measured the magnetoresistance $R_s(B)$ at fixed temperatures up to 10 K for all the bridges. In the Supplementary Figs. 3 and 4, we show representative $R_s(B)$ data from 0.35 to 3.5 K for the 1000 and 2 μm-wide bridges, respectively, where the phase boundaries are revealed by a series of crossing points, corresponding to the $T_{min}$ and $T_{max}$ plateaus on the $R_s(T)$ curves. For the 1000 μm-wide bridge, the crossing points of these $R_s(B)$ curves gradually shift from $B_c^1 = 5.42$T at low temperature to $B_c^2 = 6.4$T at $T_c(0)$, thereby defining the boundary between the superconducting and the Bose-insulating state (see phase diagram in Fig. 2a). For the 2 μm-wide bridge, by contrast, the corresponding crossing points of $R_s(B)$ curves move strongly upward for data below $\approx 1.4$K, indicating the recovery of superconductivity and an associated bending of the superconductor-to-Bose insulator phase-transition boundary at low temperature (see phase diagrams in Fig. 2b–d). The evolution of all these phase boundaries with bridge width $w$ are summarized in the Supplementary Fig. 5 and in Supplementary Movie 2. The presence of an additional fermionic channel may, in principle, lead to a small shift of the positions of the minima and maxima in

the corresponding $R(B,T)$ curves due to the temperature dependence of the respective contribution to the electrical conductivity, in comparison to a hypothetical case where this additional contribution is absent. As this temperature dependence has been shown to be weak near the SIT[8], we neither expect that the qualitative behavior of the phase boundaries shown in Fig. 2 would entirely change nor that any of these boundaries or the reported size effect completely disappear.

**Scaling analysis along the phase boundaries**. To further investigate the nature of the SITs, we use a scaling analysis on the superconductor-to-insulator phase boundaries. Near the quantum critical point, physical quantities for an equilibrium system can be classified into distinct universality classes determined only by the general properties of the system, such as space dimensionality, range and dynamics of the interactions, and symmetry, independent of the microscopic details. For a magnetic field-induced transition occurring at $B = B_c$, the experimental characteristics of the quantum critical state is the scaling behavior of physical quantities within the critical regime, showing a power-law dependence on the rescaled spatial (correlation length $\xi \propto |B - B_c|^{-\nu}$) and temporal (correlation time $\tau \propto \xi^z \propto |B - B_c|^{-z\nu}$) coordinates[17,18].

We first performed the scaling analysis on the 1000 μm-wide bridge, representing the infinitely large case, where the SIT boundary from $B_c^1$ to $B_c^2$ is constituted by a series of $T_{min}$ plateaus (Fig. 4). Near $B_c^1$, on both sides of the transition, the sheet resistance can be rescaled as $R_s(B, T) = R_c F(|B - B_c^1|T^{-1/z\nu})$, where $F(x)$ is a universal scaling function with $F(0) = 1$. By rescaling the field in Fig. 4a as $|B - B_c^1|t$, where $t = T^{-1/z\nu}$, all the $R_s(B, T)$ curves within the quantum critical regime collapse onto a single curve, as it is shown in Fig. 4b. From the rescaling factor $t$, the critical exponents $z\nu$ can be obtained by a power-law fit of $t(T)$, yielding $z\nu = 1.3331 \sim 4/3$ with high precision on both
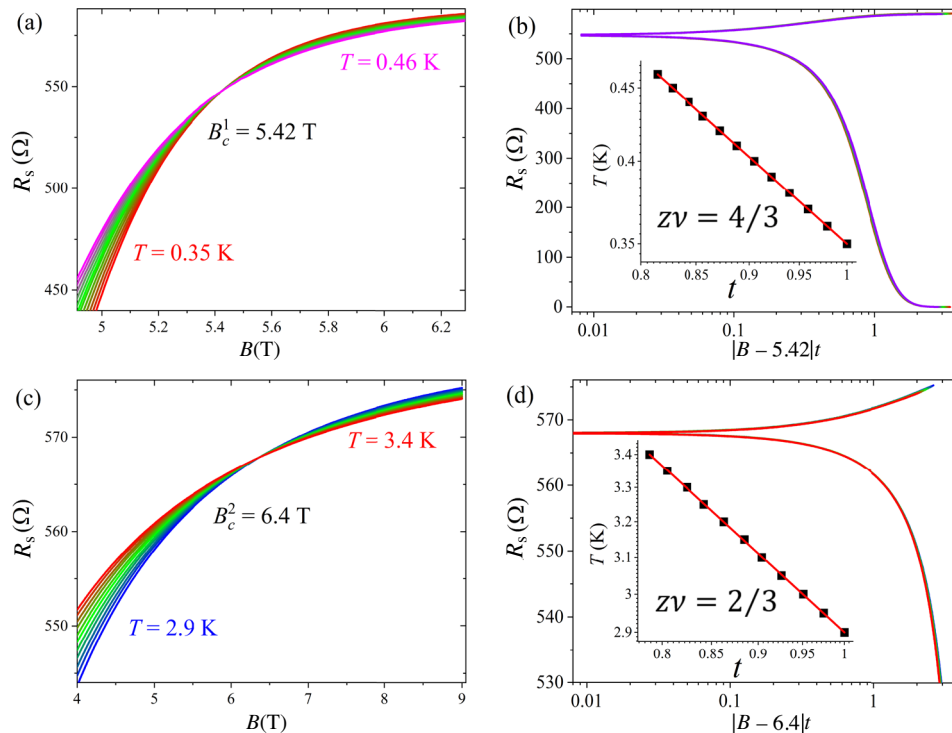
**Fig. 4 Scaling analysis on the superconductor-to-Bose insulator quantum phase transitions of the 1000 μm-wide bridge. a** Sheet resistance $R_s$ as a function of magnetic field at temperatures from 0.35 to 0.46 K, showing a distinct crossing point at the Bose insulator quantum critical field $B_c^1$. **b** Scaling-analysis plot of $R_s$ as a function of $|B - B_c^1|t$. Inset: temperature dependence of the scaling parameter $t$, with a product of the correlation length and dynamical exponents $z\nu = 4/3$. **c** $R_s(B)$ curves at temperatures from 2.9 to 3.4 K, manifesting the pair-breaking critical field $B_c^2$ near $T_c(0)$. **d** Scaling-analysis plot within the critical regime at $B_c^2$. Inset: temperature dependence of the scaling parameter $t$, with $z\nu = 2/3$.

sides of the transition. Similarly, the superconductor-to-Bose insulator quantum phase transition can also be observed in the 500 μm-wide bridge, with the same critical field value. The resulting $z\nu = 4/3$ has been observed in many 2D superconducting systems and confirms the universal behavior of the superconductor-to-Bose insulator quantum phase transitions in large 2D superconducting systems[7–9,13,14]. Performing a similar scaling analysis for the pair-breaking critical field $B_c^2(T_c)$ at temperatures between 2.9 and 3.4 K (Fig. 4c) near the finite-temperature critical point at $T_c(0)$, we obtain the best data collapse with $z\nu = 0.6667 \sim 2/3$ (Fig. 4d). These resulting critical-exponent products and the critical behavior, in general, are consistent with our previous results for infinitely large 2D bridges[14].

As for the narrow bridges, the $B_c^*$ phase boundary corresponds to the $T_{\max}(B_c^*)$ plateaus (Fig. 2b–d and Supplementary Fig. 5). In Fig. 5, we show the corresponding scaling analyses for the 2 μm-wide bridge. The first $T_{\max}(B_c^*)$ plateau appears at $B_c^* = 6.1$ T, as it is shown in Fig. 5a, at temperatures between 1.18 and 1.34 K. By utilizing the scaling analysis, the $R_s(B)$ data within the critical regime are perfectly rescaled onto a single curve, as it is shown in Fig. 5b, resulting in a product of the critical exponents $z\nu = 0.7365$. The largest critical point that could be investigated with our equipment is $B_c^* = 7.1$ T (shown in Fig. 5c, at temperatures from 0.34 to 0.45 K). The best data collapse yields a relatively large critical-exponent product of 2.3443 (Fig. 5d). To reveal the effects of the bridge dimensions on the critical behavior, we performed corresponding scaling analyses every 0.1 T for all the bridges (details about the scaling analysis procedure at the $B_c^*(T_{\max})$ boundary are shown in the Supplementary Fig. 6) and the resulting field dependences of $z\nu$ for these bridges are summarized in Fig. 6. Different from the superconductor-to-Bose

insulator phase transitions in large 2D systems, in which $z\nu$ lies between 2/3 and 4/3[14], the product $z\nu$ at the $B_c^*(T_{\max})$ boundary grows dramatically with increasing magnetic field and it is expected to diverge at the zero-temperature superconductor-to-Fermi insulator quantum critical point at $B_c^*(0) = B_c^F$, thereby revealing the signature of a quantum Griffiths singularity[27–33].

Inspired by the activated scaling law for the quantum Griffiths singularity[27], we fitted the extracted $z\nu$ for all the bridges according to $z\nu = C \cdot \left(B_c^F - B_c^*\right)^{-\nu\Psi}$ (solid lines in Fig. 6; the fitting results are summarized in Supplementary Table 1). The resulting critical-exponent products $\nu\Psi$ are close to 0.6 only for 2 and 3 μm-wide bridges. For the relatively wide bridges, the $\nu\Psi$ strongly depend on the bridge width, which can be attributed to the different levels of quenched disorder in the different bridges as we will outline further below. The most remarkable result of this fitting procedure is that the resulting $B_c^F = B_c^*(0)$ values for all bridges are around $7.25 \pm 0.01$ T. This size-independent field $B_c^F$ represents the highest magnetic field in which Cooper pairs can still exist in the films in the zero-temperature limit. It therefore corresponds to the zero-temperature quantum critical field for the direct superconductor-to-Fermi insulator quantum phase transitions for narrow-enough bridges, irrespective of the geometries of the superconducting structures.

**Decisive role of the system size.** The physical origin of the seemingly contradictory nature of the phase transitions in the different bridges can be understood in the context of vortex physics. In superconducting thin films, vortices interact via their stray fields in the surrounding space, different from their bulk peers[42]. The stray field in a 2D system is mainly mediated by the effective penetration depth $\Lambda = 2\lambda_L^2/d$, with $\lambda_L$ the London penetration
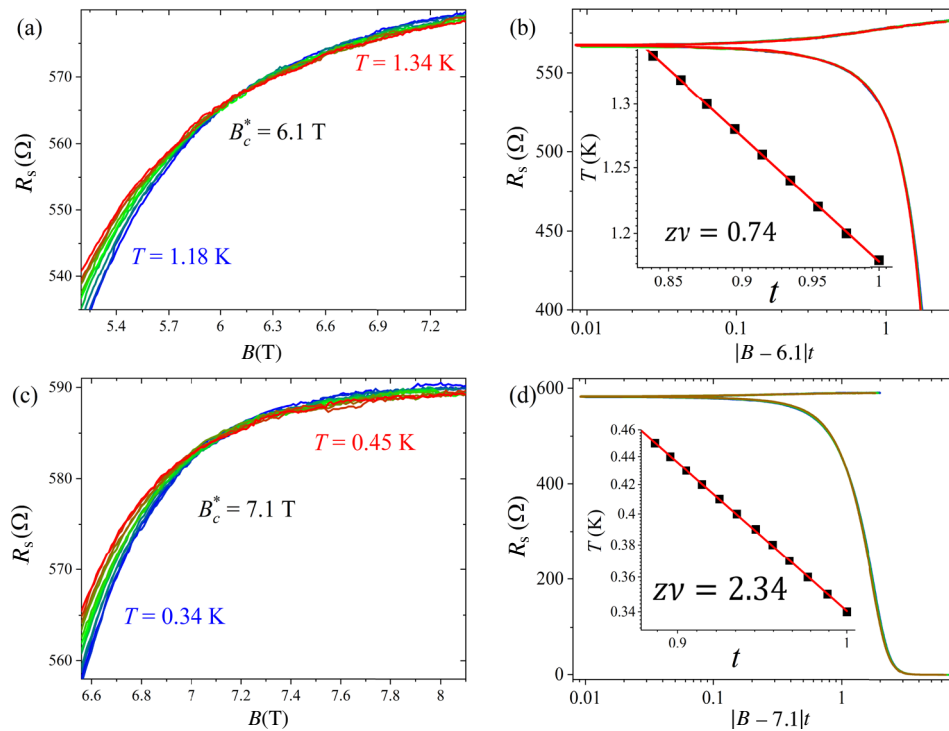
**Fig. 5 Scaling analysis on the superconductor-to-insulator quantum phase transitions of the 2 μm-wide bridge. a** Sheet resistance $R_s$ as a function of magnetic field at temperatures between 1.18 and 1.34 K, showing a distinct crossing point of the first $T_{max}$ plateau at the re-entrance field to superconductivity $B_c^* = 6.1$ T. **b** Scaling-analysis plot of $R_s$ as a function of $|B - 6.1|t$. Inset: temperature dependence of the scaling parameter $t$, with a product of the correlation length and dynamical exponents $z\nu = 0.7365$. **c** Sheet resistance as a function of field $R_s(B)$ at temperatures between 0.34 and 0.45 K, showing the crossing point of the $T_{max}$ plateau at $B_c^* = 7.1$ T. **d** Scaling-analysis plot within the critical regime at 7.1 T. Inset: temperature dependence of the scaling parameter $t$, with $z\nu = 2.3443$.
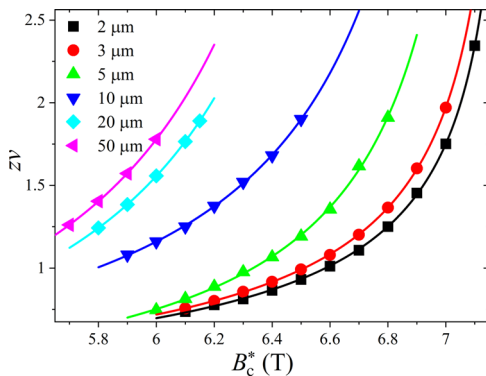


**Fig. 6 The scaling behavior of the product of the correlation length and dynamical exponents $z\nu$ as a function of the re-entrance field to superconductivity $B_c^*$ for narrow bridges.** The solid lines represent fits according to the activated scaling law $z\nu = C \cdot \left(B_c^F - B_c^*\right)^{-\nu\Psi}$, with $B_c^F = 7.25$ T the Fermi insulator quantum critical field, $\nu\Psi$ the critical-exponent product characterizing the divergence at a quantum Griffiths singularity, and $C$ a pre-factor.

depth, which is $\Lambda(0) \approx 350$ μm in our case[36,37]. For an infinitely large 2D superconducting thin film in a strong magnetic field, vortices localize due to the long-range logarithmic repulsive interactions $V_{int} \propto \ln(\Lambda/r)$, where $r$ is the distance between two vortices. As a result, field-induced vortices freeze into a regular vortex lattice in the zero-temperature limit, underlying the global coherence, and the zero-resistivity state survives at first in a strong magnetic field. When the magnetic field is increased further, the vortices eventually condense (i.e., delocalize) at a critical

field $B_c^l$, in analogy to the condensation of Cooper pairs and the localization of vortices in the superconducting state[17,18]. Although global superconducting coherence is then destroyed, isolated superconducting islands remain, with mobile vortices that are induced by quantum phase fluctuations[17–20]. This transition can be regarded as a quantum analog of the vortex unbinding-induced Kosterlitz–Thouless transition. In short, the quantum nature of the superconductor-to-Bose insulator quantum phase transition in sufficiently wide structures corresponds to the delocalization of vortices and the localization of Cooper pairs, accompanied by the loss of the global coherence[17,18].

The interaction between vortices can, however, change from long range to an exponentially weak and short-range interaction along the bridge as soon as the characteristic length scale of the superconducting system is smaller than $\Lambda(0)$[43,44]. This may prohibit the formation of a long-range ordered vortex lattice. As we recently demonstrated in similar superconducting microbridges[37], an extra pinning effect for bridge widths smaller than $\Lambda(0)$ prohibits the vortices from moving, leading to a strong suppression of the resistivity even near the normal-to-superconductor transition at the critical temperature $T_c(B)$ (see also Supplementary Fig. 7). Upon approaching the zero-temperature limit, where thermal fluctuation effects on the vortices are negligible, the initially mobile vortices in the Bose-insulating state freeze again due to this size effect in the narrow bridges, which leads to a dramatic decrease in resistivity and the recovery of superconductivity. Within this line of arguments, vortices do not constitute a long-range ordered vortex lattice in bridges with dimensions smaller than $\Lambda(0)$. Instead, they are prone to form locally ordered regions, which are connected by disordered and randomly located vortices with quenched

disorder, leading to a vortex-glass-like state near $B_c^F$, as schematically illustrated in ref. [34]. The disorder level of the vortex-glass-like state in narrow bridges therefore intrinsically strongly depends on the bridge width $w$, even if these bridges exhibit the same quality of the underlying superconducting film. This is in contrast to cases where the level of disorder of the vortex ensemble in a film is dictated by external parameters such as local defects or any other irregularities. At any rate, this vortex-glass-like state breaks the transitional and rotational symmetry of the vortex lattice, and dramatically alters the nature of the transition, manifesting itself in a quantum Griffiths singularity[34]. A direct superconductor-to-Fermi insulator quantum phase transition due to the direct Cooper pair breaking eventually occurs at the critical field $B_c^F$ in the zero-temperature limit. Such a quantum Griffiths singularity in superconducting systems should always be observed as soon as the quenched disorder plays an important role near the quantum critical point.

## Conclusion

Our key experimental findings are shown in the schematic $B$–$T$ phase diagrams in Fig. 2 (see Supplementary Figs. 8 and 9 for a summary of the corresponding $R_s(T)$ data for different magnetic fields; the Supplementary Fig. 5 and Supplementary Movie 2 summarize the phase diagrams for all bridges). The Fig. 2a represents the sequential superconductor–Bose insulator–Fermi insulator quantum phase transitions for infinite films $w \gg \Lambda(0)$, where $B_c^1$ is the critical field for the localization of Cooper pairs and $B_c^2$ is the highest field in which Cooper pairs can persist in the films at $T_c(0)$. The ultimate pair-breaking field of localized pairs in the Bose-insulating state is represented by the dashed line. The superconductor-to-Bose insulator quantum phase transition should be universal to all infinite 2D superconducting systems with intrinsically weak vortex pinning. In the language of vortices, the vortex lattice is static and contiguous below $B_c^1$ at zero temperature, as a manifestation of global phase coherence. Upon crossing $B_c^1$, it may "quantum melt" in the spirit of ref. [18]. As soon as the bridge width is narrower than the Pearl length $\Lambda(0)$, but still much larger than the coherence length $\xi(0) \approx 8$ nm[37], superconductivity is recovered from the Bose-insulating state, because a reduction of the bridge width alters the vortex–vortex interaction to short range and the vortices become prone to pinning. This increased tendency to pinning may then hinder the quantum melting in the narrow bridges at low temperatures and push the boundary between the superconducting and the Bose-insulating phase to higher fields. At $T = 0$, we even expect a direct superconductor-to-Fermi insulator transition. At finite temperatures $T > 0$, however, the Bose-insulating phase shrinks with decreasing bridge width, terminating at $B_c^F = 7.25$T, but it exists up to $T_c(0)$ at $B_c^2$ for all bridges (see Supplementary Fig. 10). By further reducing the bridge width towards the 1D limit, we suppose that the Bose-insulating state will eventually entirely disappear (Fig. 2f), so that the phase diagram is divided into only two distinct regions (with $\partial R_s/\partial T > 0$ and $\partial R_s/\partial T < 0$, respectively), as it is observed for a quantum Griffiths singularity[27–33]. A direct superconductor-to-Fermi insulator phase transition occurs at all temperatures up to $T_c(0)$ and beyond, as long as superconducting fluctuations are still present. As the recovery of superconductivity and the appearance of a quantum Griffiths singularity in the zero-temperature limit in narrow-enough bridges are most probably due to a size-effect-induced disorder and a resulting breaking of transitional and rotational symmetry of the vortex lattice, a quantum Griffiths singularity should be universally expected in sub-2D superconducting systems with characteristic dimensions smaller than the Pearl length $\Lambda(0)$. Our experimental findings may solve part of the controversy concerning the nature of magnetic field-driven superconductor-to-insulator quantum phase transitions in 2D superconducting systems.

## Methods

The superconducting thin films adopted in our research were prepared by magnetron sputtering deposition. The WSi films were deposited by co-sputtering from W and Si targets in 1.2 mTorr Ar pressure on an oxidized Si substrate. The sputtering powers for W and Si guns were 100 and 180 W, respectively. The WSi film was in situ capped with a 2 nm sputtered amorphous Si film. The WSi film had a nominal Si content of ~25% and showed an amorphous structure as verified by X-ray diffraction and cross-sectional transmission electron microscopy.

We at first patterned Ti/Au (with thicknesses of 2 and 100 nm, respectively) contacts on the as-grown films by lift-off technique. Then the microbridges were defined by optical lithography, followed by reactive ion-etching. The bridge widths range from 2 to 1000 μm. To exclude to any possible formation of pinning centers by high-energy electron irradiation, we here only applied optical lithography to fabricate these bridges instead of electron-beam lithography. The bridge length was and 3000 μm-long for the 1000 and the 500 μm-wide bridges, respectively. For all other bridges, the length was 800 μm. Images of similar microbridges can be found in ref. [36]. The contacts were fabricated using a wire bonder in a four-point probing configuration and with aluminum wires attached to the gold layer, with a contact resistance of the order of a few Ohms. The resistivity measurements were done in a Physical Property Measurement System (Quantum Design, Inc.) equipped with a $^3$He option. All measurements were performed with the same current density $j = 1.25$ MA m$^{-2}$. The bias currents were therefore ranging from 10 nA (for the 2 μm-wide bridge) to 5 μA (for the 1000 μm-wide bridge).

Weakly-pinning amorphous superconductors, such as WSi, InO$_x$, and MoGe, are the most optimal platforms for investigating the quantum nature of superconductor-to-insulator quantum phase transitions, the details of which depend on the intrinsic interactions among vortices. In the strongly pinning peers, such as NbN, the pinning centers inside the materials prevent vortices from freely moving, making the interactions between free vortices inaccessible. Although atomically ordered superconducting crystalline films such as exfoliated NbSe$_2$ monolayers are also perfect candidates, the generally available thin flakes usually have limited size and the effective penetration depth can be several orders of magnitude larger than the flake size, so that the limit $w > \Lambda(0)$ can hardly be achieved.

## Data availability

All data needed to evaluate the conclusions in the paper are present in the paper and/or the Supplementary Information. The data that support the findings of this study are available from the corresponding authors upon reasonable request.

## References

1. Bardeen, J., Cooper, L. N. & Schrieffer, J. R. Theory of superconductivity. *Phys. Rev.* **108**, 1175–1204 (1957).
2. Rasolt, M. & Tešanović, Z. Theoretical aspects of superconductivity in very high magnetic fields. *Rev. Mod. Phys.* **64**, 709–754 (1992).
3. Goldman, A. M. Superconductor-insulator transitions. *Int. J. Mod. Phys. B* **24**, 4081–4101 (2010).
4. Gantmakher, V. F. & Dolgopolov, V. T. Superconductor–insulator quantum phase transition. *Phys. Usp.* **53**, 1–49 (2010).
5. Sacépé, B., Feigel'man, M. & Klapwijk, T. M. Quantum breakdown of superconductivity in low-dimensional materials. *Nat. Phys.* **16**, 734–746 (2020).
6. Haviland, D. B., Liu, Y. & Goldman, A. M. Onset of superconductivity in the two-dimensional limit. *Phys. Rev. Lett.* **62**, 2180–2183 (1989).
7. Hebard, A. F. & Paalanen, M. A. Magnetic-field-tuned superconductor–insulator transition in two-dimensional films. *Phys. Rev. Lett.* **65**, 927–930 (1990).
8. Yazdani, A. & Kapitulnik, A. Superconducting–insulating transition in two-dimensional a-MoGe thin films. *Phys. Rev. Lett.* **74**, 3037–3040 (1995).
9. Mason, N. & Kapitulnik, N. Dissipation effects on the superconductor-insulator transition in 2D superconductors. *Phys. Rev. Lett.* **82**, 5341–5344 (1999).
10. Marković, N., Christiansen, C. & Goldman, A. Thickness-magnetic field phase diagram at the superconductor–insulator transition in 2D. *Phys. Rev. Lett.* **81**, 5217–5220 (1998).
11. Aubin, H. et al. Magnetic-field-induced quantum superconductor–insulator transition in Nb$_{0.15}$Si$_{0.85}$. *Phys. Rev. B* **73**, 094521 (2006).
12. Biscaras, J. et al. Multiple quantum criticality in a two-dimensional superconductor. *Nat. Mater.* **12**, 542–548 (2013).
13. Shi, X., Lin, P. & Sasagawa, T. Two-stage magnetic-field-tuned superconductorinsulator transition in underdoped La$_{2-x}$Sr$_x$CuO$_4$. *Nat. Phys.* **10**, 437–443 (2014).

14. Zhang, X. & Schilling, A. Sequential superconductor–Bose insulator–Fermi insulator phase transitions in quasi-two-dimensional $a$-WSi. *Phys. Rev. B* **97**, 214524 (2018).

15. Lu, X. et al. Superconductors, orbital magnets and correlated states in magic-angle bilayer graphene. *Nature* **574**, 653–657 (2019).

16. Yu, Y. et al. High-temperature superconductivity in monolayer $Bi_2Sr_2CaCu_2O_{8+\delta}$. *Nature* **575**, 156–163 (2019).

17. Fisher, M. P., Weichman, P. B., Grinstein, G., & Fisher, D. S. Boson localization and the superfluid-insulator transition. *Phys. Rev. B Condens. Matter* **40**, 546–570 (1989).

18. Fisher, M. P. A. Quantum phase transitions in disordered two-dimensional superconductors. *Phys. Rev. Lett.* **65**, 923–926 (1990).

19. Phillips, P. & Dalidovich, D. The elusive Bose metal. *Science* **302**, 243–247 (2003).

20. Phillips, P. Two-dimensional materials: not just a phase. *Nat. Phys.* **12**, 206–207 (2016).

21. Valles, J. M., Dynes, R. C. & Garno, J. P. Electron tunneling determination of the order-parameter amplitude at the superconductor-insulator transition in 2D. *Phys. Rev. Lett.* **69**, 3567–3570 (1992).

22. Hsu, S. Y., Chervenak, J. A. & Valles, J. M. Jr. Magnetic field enhanced order parameter amplitude fluctuations in ultrathin films near the superconductor-insulator transition. *Phys. Rev. Lett.* **75**, 132–135 (1995).

23. Szabó, P. et al. Fermionic scenario for the destruction of superconductivity in ultrathin MoC films evidenced by STM measurements. *Phys. Rev. B* **93**, 014505 (2016).

24. Allain, A., Han, Z. & Bouchiat, V. Electrical control of the superconducting-to-insulating transition in graphene-metal hybrids. *Nat. Mater.* **11**, 590–594 (2012).

25. Bollinger, A. T. et al. Superconductor–insulator transition in $La_{2-x}Sr_xCuO_4$ at the pair quantum resistance. *Nature* **472**, 458–460 (2011).

26. Caviglia, A. D. et al. Electric field control of the $LaAlO_3/SrTiO_3$ interface ground state. *Nature* **456**, 624–627 (2008).

27. Xing, Y. et al. Quantum Griffiths singularity of superconductor-metal transition in Ga thin films. *Science* **350**, 542 (2015).

28. Xing, Y. et al. Ising superconductivity and quantum phase transition in macrosize monolayer NbSe$_2$. *Nano Lett.* **17**, 6802 (2017).

29. Shen, S. et al. Observation of quantum Griffiths singularity and ferromagnetism at the superconducting $LaAlO_3/SrTiO_3$(110) interface. *Phys. Rev. B* **94**, 144517 (2016).

30. Saito, Y., Nojima, T. & Iwasa, Y. Quantum phase transitions in highly crystalline two-dimensional superconductors. *Nat. Commun.* **9**, 778 (2018).

31. Liu, Y. et al. Anomalous quantum Griffiths singularity in ultrathin crystalline lead films. *Nat. Commun.* **10**, 1–6 (2019).

32. Zhang, E. et al. Signature of quantum Griffiths singularity state in a layered quasi-one-dimensional superconductor. *Nat. Commun.* **9**, 4656 (2018).

33. Lewellyn, N. A. et al. Infinite-randomness fixed point of the quantum superconductor-metal transitions in amorphous thin films. *Phys. Rev. B* **99**, 054515 (2019).

34. Markovic, N. Randomness rules. *Science* **350**, 509–509 (2015).

35. Saito, Y., Nojima, T. & Iwasa, Y. Highly crystalline 2D superconductors. *Nat. Rev. Mater.* **2**, 16094 (2016).

36. Zhang, X. et al. Superconducting fluctuations and characteristic time scales in amorphous WSi. *Phys. Rev. B* **97**, 174502 (2018).

37. Zhang, X. et al. Strong suppression of the resistivity near the superconducting transition in narrow microbridges in external magnetic fields. *Phys. Rev. B* **101**, 060508 (2020).

38. Žemlička, M. et al. Zeeman-driven superconductor-insulator transition in strongly disordered MoC films: scanning tunneling microscopy and transport studies in a transverse magnetic field. *Phys. Rev. B* **102**, 180508(R) (2020).

39. Sacépé, B. et al. Disorder-induced inhomogeneities of the superconducting state close to the superconductor-insulator transition. *Phys. Rev. Lett.* **101**, 157006 (2008).

40. Ganguly, R. et al. Magnetic field induced emergent inhomogeneity in a superconducting film with weak and homogeneous disorder. *Phys. Rev. B* **96**, 054509 (2017).

41. Šimánek, E. Reentrant phase transition of granular superconductors. *Phys. Rev. B* **23**, 5762 (1981).

42. Pearl, J. Current distribution in superconducting films carrying quantized fluxoids. *Appl. Phys. Lett.* **5**, 65–66 (1964).

43. Kogan, V. G. Pearl's vortex near the film edge. *Phys. Rev. B* **49**, 15874–15878 (1994).

44. Kogan, V. G. Interaction of vortices in thin superconducting films and the Berezinskii-Kosterlitz-Thouless transition. *Phys. Rev. B* **75**, 064514 (2007).

## Acknowledgements

## Author contributions

X.Z. and A.S. conceived the research. A.E.L., V.B.V., and S.W.N. deposited the films. X.Z. fabricated the devices and performed all the measurements. X.Z., H.L., Q.Z., and A.S. analyzed the data and wrote the paper.

## Competing interests

The authors declare no competing interests.

## Additional information

**Supplementary information** The online version contains supplementary material available at https://doi.org/10.1038/s42005-021-00602-7.

**Correspondence** and requests for materials should be addressed to X.Z. or A.S.

**Reprints and permission information** is available at http://www.nature.com/reprints

**Publisher's note** Springer Nature remains neutral with regard to jurisdictional claims in published maps and institutional affiliations.